

Computing bluff body flows using commercial CFD software

Sujit Kirpekar and David B. Bogy

Computer Mechanics Laboratory

Department of Mechanical Engineering

University of California at Berkeley

Berkeley, CA 94720

Telephone: (510)642-4975

Fax: (510)643-9786

`kirpekar@newton.berkeley.edu`

July 18, 2005

Contents

1	Introduction	1
2	Configuration and Setup	3
3	Results and Discussion	6
3.1	Global Quantities	7
3.2	Time-Averaged Quantities	9
3.3	Phase Averaged Quantities	10
4	The Effect of Upwind differencing	13
5	Concluding Remarks	15
6	Tables	20
7	Figures	22

List of Figures

1	Model Configuration and Setup	22
2	Cross Section of the Grid	22
3	Time averaged streamwise velocity	23
4	Time averaged RMS streamwise velocity	23
5	Time averaged RMS vertical velocity	23
6	Time averaged Reynolds stress component, $\langle u'v' \rangle$	23
7	Streamlines for Phase 01, ACE1	24
8	Streamlines for Phase 01, ACE2	24
9	Streamlines for Phase 01, ACE3	24
10	Streamlines for Phase 01, Flu1	24
11	Streamlines for Phase 01, Flu2	25
12	Streamlines for Phase 01, Flu3	25
13	Streamlines for Phase 01, from Lyn and Rodi (1994)	25
14	Streamlines for Phase 01, from Lakehal and Thiele (2001)	25
15	Streamlines for Phase 09, ACE1	26
16	Streamlines for Phase 09, ACE2	26
17	Streamlines for Phase 09, ACE3	26
18	Streamlines for Phase 09, Flu1	26
19	Streamlines for Phase 09, Flu2	27
20	Streamlines for Phase 09, Flu3	27
21	Streamlines for Phase 09, from Lyn and Rodi (1994)	27
22	Streamlines for Phase 09, from Lakehal and Thiele (2001)	27
23	Phase averaged vertical velocity for Phase 01	28
24	Phase averaged vertical velocity for Phase 09	28

25	Phase averaged vertical velocity for Phase 05	28
26	Phase averaged vertical velocity for Phase 15	28
27	Comparison of time averaged streamwise velocity between ACE1 and ACE1 with 10% upwind differencing	29
28	Comparison of time averaged streamwise velocity between ACE2 and ACE2 with 10% upwind differencing	29
29	Comparison of time averaged RMS streamwise velocity between ACE1 and ACE1 with 10% upwind differencing	29
30	Comparison of time averaged RMS streamwise velocity between ACE2 and ACE2 with 10% upwind differencing	29
31	Comparison of time averaged RMS vertical velocity between ACE1 and ACE1 with 10% upwind differencing	30
32	Comparison of time averaged RMS vertical velocity between ACE2 and ACE2 with 10% upwind differencing	30
33	Streamlines for Phase 01, ACE1	31
34	Streamlines for Phase 01, ACE1 with 10% upwinding	31
35	Streamlines for Phase 01, ACE2	31
36	Streamlines for Phase 01, ACE2 with 10% upwinding	31
37	Streamlines for Phase 09, ACE1	32
38	Streamlines for Phase 09, ACE1 with 10% upwinding	32
39	Streamlines for Phase 09, ACE2	32
40	Streamlines for Phase 09, ACE2 with 10% upwinding	32

List of Tables

1	Global Results	20
2	Common Legend for Figures	21
3	The effect of 10% upwind differencing	21

Abstract

The ability of three commercial codes, CFD-ACE v2004, Fluent 6.2.16 and CFX 5.7.1 to compute the flow over a bluff body is examined. Large Eddy Simulation (LES) is used to compute the flow across a square prism using four different SGS models implemented in these commercial codes: the Smagorinsky's model (Smagorinsky, 1963), the dynamic model (Germano et al., 1991), the localized dynamic model (Kim and Menon, 1995) and the WALE model (Nicoud and Ducros, 1999). Global simulation results, time averaged quantities and phase averaged quantities are benchmarked against the experimental results of Lyn and Rodi (1994). All simulations predict the Strouhal number fairly accurately, and simulations employing the dynamic model are excellent in predicting the mean recirculation length and the r.m.s. of the lift coefficient on the prism. In terms of flow fluctuations, all simulations over-predict the streamwise component, but under-predict the vertical component. Velocity fluctuations in the wake correlate well with the fluctuation of forces on the prism. An examination of the streamlines of the flow indicates again that CFD-ACE and Fluent's implementation of the dynamic model offers the best prediction of the vertical displacement of the wake and the size of the shed vortex. It is also observed that Smagorinsky's model implemented in CFX delivers a poor prediction of the flow compared with CFD-ACE and Fluent's implementations of the same model. Finally, the addition of 10% up-wind differencing to the convective terms is shown to cause an artificial increase in the lift fluctuation. This effect is more pronounced in the dynamic model than in the Smagorinsky's model.

1 Introduction

Engineering calculations of flows in complex geometries are often presented without any verification or validation, in spite of being most susceptible to errors. (Validation is defined

(Stern et al., 2001) as “*a process for ascertaining simulation modeling uncertainty by using benchmark experimental data and, when conditions permit, estimating the sign and magnitude of the modeling error itself*”). Moreover, commercial CFD codes used in industrial applications are efficient in calculating results, but do not offer insights into the numerical uncertainties of those results. In this light, large eddy simulation (LES) results of the flow across a square prism are presented using three commercial codes, and four different subgrid scale (SGS) models.

The original problem of interest to the authors is the flow of air in hard disk drive enclosures. Such flows are highly complex and little experimental data is available for comparison¹. When experimental data is limited, a common practice is to use the commercial code to solve a well known test case for which a rich set of experimental data is available. This often helps in highlighting the merits and demerits of the software. The test case chosen here (the flow across a square prism) has several similarities with the original problem of interest. Both flows have a blunt body obstruction, massive flow separation, formation of a “flapping” shear layer, regions of laminar, transitional and turbulent flow, recirculation, vortex shedding and an inherent three dimensional nature.

In a CFD Biathlon Forum (Freitas, 1995), several commercial codes were tested (including CFD-ACE and Fluent) in solving five model problems. The flow across a square prism was a part of tests, but only 2-dimensional simulations using RANS models were presented. Several LES codes were used to solve the square prism case during a workshop held in Germany in June 1995 (Rodi et al., 1997). Similarly, at the ERCOFTAC Workshop, seven groups submitted their time-averaged solutions of the problem; The results are published in Voke (1997). In addition to these workshops, there is a wealth of literature discussing the application of LES to this problem. Among the most recent works is that of Sohankar

¹In a separate work the authors are validating their LES results for flows in disk drives with the experimental results of Gross (2003)

et al. (2000), who tested three SGS models and varied other parameters such as the grid size, time step and spanwise dimension. Fureby et al. (2000) also tested several SGS models and generated a database of first and second order statistical moments of the resolved velocity.

Most of the cited literature above use codes that were developed by university researchers, but there exist (to the authors knowledge) no such published tests on commercial codes. The main objective of the current work is to investigate the ability of three commercial codes to solve the square prism problem: CFD-ACE 2004, Fluent 6.2.16 and CFX 5.7.1,(and their implementations of four SGS models: the Smagorinsky’s model (Smagorinsky, 1963), the (Algebraic) dynamic model (Germano et al., 1991), the localized dynamic one-equation model (Kim and Menon, 1995) and the wall-adapting local eddy-viscosity (WALE) model (Nicoud and Ducros, 1999)). Such a comparison between the simulation results from different commercial codes serves as an effective test of the internal numerics of the code, which are usually hidden from the user (e.g. segregated v/s coupled solvers, convergence criteria for each time step, under-relaxation parameters, artificially imposed bounds or limiters, etc).

2 Configuration and Setup

A two-dimensional schematic plan view drawing of the problem geometry is shown in Figure 1. In Cartesian coordinates, the origin is located at the center of the prism, the mean flow is oriented in the x-direction, and Figure 1 depicts a representative $x - z$ plane. The side of the square prism is (in the streamwise direction) d and the inflow x-velocity is U_∞ . Henceforth, as is traditional, all dimensions are scaled by d , all velocities by U_∞ and times by d/U_∞ .

The Reynolds number of the flow ($Re = \frac{U_\infty d}{\nu}$) was 22,000, the upstream distance, X_u was 4.5, while the downstream distance X_d was 15. The lateral dimension H was 4, while the dimension in the y-direction was 14. All of the simulations used the same grid, consisting of

$165 \times 105 \times 25$ cells, an $x - y$ plane of which is shown in Figure 2. The distribution of nodes was uniform outside a region extending two units upstream, downstream and sideways (in the y -direction) of the prism (as in Sohankar et al. (2000)). The uniform cell spacing was 0.167 downstream (Δx_d), 0.25 upstream (Δx_u) and 0.167 in the z -direction (Δz), again as in Sohankar et al. (2000). In the region of the grid close to the prism, a hyperbolic tangent function was used to stretch the cells. The first node away from the prism wall was at a distance of 0.00815 in both x - and y - directions.

CFD-ACE and Fluent codes are based on the incompressible cell-centered finite volume formulation. The governing system was solved iteratively using the SIMPLEC technique (originally due to Van doormaal and Raithby, 1984) (i.e. they use segregated solvers), although other methods (e.g. PISO) were available in Fluent. On the other hand, CFX employs a pressure based coupled solver. A preconditioned multigrid method is used to solve the linear system arising from the coupled Navier Stokes and continuity equations. For further details on the solution strategies of each software, we refer the reader to their respective user manuals. Seven simulations were computed:

1. CFD-ACE using the Smagorinsky model (ACE1)
2. CFD-ACE using the dynamic model (ACE2)
3. CFD-ACE using the localized dynamic model (ACE3)
4. Fluent using the Smagorinsky model (Flu1)
5. Fluent using the dynamic model (Flu2)
6. Fluent using the WALE model (Flu3), and,
7. CFX using the Smagorinsky model (CFX1) ²

²The Smagorinsky model was the only SGS model available in CFX.

A description of the above SGS models is not provided here. The reader is referred to Kirpekar and Bogy (2004) for details on these common SGS models. Simulations ACE1, Flu1 and CFX1 used $C_s = 0.1$ for the Smagorinsky’s model. In simulation Flu2, the value of C_s was clipped below 0 and above 0.23. And in simulation Flu3, the parameter C_ω of the WALE model was set to 0.325.

All simulations used centered differencing for the convective terms, to avoid the well known diffusion associated with upwind biased schemes. The effect of adding a small amount of upwind-biased differencing is discussed later in Section 4. All CFD-ACE simulations used the first order Implicit Euler’s method for time advancement. A semi-implicit second order method (Crank Nicholson) was available in CFD-ACE, but calculations using it would become unstable as time progressed. All Fluent simulations and the CFX simulation used a two step BDF method which is second order accurate and provides better stiff stability than corresponding implicit Adams methods (This method is also known as BDF2 or Second Order Implicit Euler). For both Fluent and CFX, it not not clear from their user manuals how these 2 step step methods are started.

The inflow boundary condition was specified to be a constant inflow in the x-direction ($u = U_\infty$, $v = 0$, $w = 0$), perturbed with 2% turbulent fluctuations. In Fluent the “spectral synthesizer” model (based on Smirnov et al., 2001) was used to model the velocity fluctuations. At the outflow, convective boundary conditions, of the form,

$$\frac{\partial u_i}{\partial t} + U_\infty \frac{\partial u_i}{\partial x} = 0 \quad i = 1, 2, 3, \quad (1)$$

were used. Symmetry conditions simulating a frictionless wall,

$$u_n = \left(\frac{\partial u_i}{\partial n} \right)_{i \neq n} = 0, \quad (2)$$

were used for all the exterior lateral walls, where n is the normal direction to the wall.

The prism wall was modeled as a no-slip boundary in all simulations. None of the simulations used wall functions and the coarseness of the grid did not allow the very small turbulent structures near the wall to be resolved. Simulations ACE1 and CFX1 used the standard Van Driest (1956) damping modification for the Smagorinsky parameter C_s near the wall. Flu1 and Flu2 used a “damped mixing length” near the wall, such that for the Smagorinsky’s model constant, $C_s = \min(\kappa y_{\text{wall}}, 0.1\Delta)$, where κ is the von Kármán constant and Δ is the filter width. The other simulations, ACE2, ACE3 and Flu3 did not use any near wall modeling. All simulations used implicit grid filtering for the Smagorinsky’s models, and used a top-hat filter (which is anisotropic and inhomogeneous) for test filtering in the dynamic models, whose size was twice the grid filter.

3 Results and Discussion

All simulations were started from the initial conditions of rest and ran for at least 8 shedding cycles, identified by the time history of the lift. Coherent vortex shedding started after approximately 500 time steps. Flu1, Flu2, Flu3 and CFX1 were computed on local desktop Pentium machines, while ACE1, ACE2 and ACE3 were computed on a parallel cluster using 8 processors.

Two sets of results are presented in this paper: time-averaged and phase averaged. Phase averaged data was not available for CFX1, hence only time-averaged data will be presented for it. Time averaging was done only over complete shedding cycles i.e. initial start up data was ignored. Phase averaged data is presented by breaking up each shedding cycle into twenty phases, as in Lyn and Rodi (1994) and Lyn et al. (1995).

3.1 Global Quantities

Table 1 reports global quantities of the flow. $St = \frac{fd}{U_\infty}$ is the Strouhal number, l_r is the time-averaged recirculation length (calculated from the prism center), $\bar{C}_D, C'_D, \bar{C}_L, C'_L$ are the mean and r.m.s. values of the coefficients of drag and lift on the prism, respectively. Some authors (of both numerical and experimental works) choose to report global quantities corrected for blockage effects ((Sohankar et al., 2000), Bearman and Obasaju (1982)). However, both LES workshops (Rodi et al. (1997) and Voke (1997)) do not present blockage-corrected results, and this custom is followed here also. It should be noted that obtaining blockage-corrected values from the results presented here is a straightforward exercise, given that blockage parameter is 7.1% (the ratio of the projected area of the prism to the area of the empty channel).

Table 1 includes results from our test cases (ACE1 to CFX1) and results from several experimental investigations. Although some of the experiments used vastly different Reynolds numbers, a rough comparison still holds, based on the grounds that non-dimensional quantities like force coefficients are independent of the Reynolds number once the Reynolds number is above 20,000 (McLean and Gartshore, 1992). Also included are three representative results from the LES workshop in Germany (Rodi et al., 1997) and direct numerical simulation (DNS) result from the workshop by Voke (1997).

It appears that all our simulations are accurate in predicting the Strouhal number, while not being accurate in other quantities, which confirms the idea that the Strouhal number is insensitive to the SGS model. The mean recirculation length, which is an important quantity that determines the average size of the wake is computed from the time-averaged streamwise velocity profiles. As will be evident from the velocity profile itself, Flu2 and ACE2 most accurately predict l_r . Flu2 is the better of the two predictions, while the worst result is from CFX1. All simulations overpredict the mean drag coefficient when compared to the experiments, but the dynamic models (ACE2, ACE3 and Flu2), which do not use

any near-wall damping, are better at predicting the mean drag than the Smagorinsky's models. Generally it is expected that the recirculation length and the mean drag coefficient are inversely proportional, but the mean drag values are close to each other, and a clear trend is not manifested. It is also known (due to Lee, 1975) that increasing the free stream turbulence decreases the mean drag. Even though all the experimental results are for free streams which are *smooth* and relatively lesser turbulent (except Lyn and Rodi (1994) which report 2% upstream turbulence), our simulations predict a higher mean drag. With the exception of ACE2, ACE3 and CFX1, there is good agreement in the r.m.s. drag coefficient, while the mean lift coefficient (which should be zero due to symmetry) is appropriately close to zero in all simulations. For flow structure interaction problems, it is crucial to predict the r.m.s lift coefficient accurately. Generally the r.m.s lift coefficient is determined by the vortex dynamics of the wake since the lift is directly related to changes in circulation around the prism. The dynamic models, ACE2 and Flu2, again appear to provide impressive results, with ACE2 the better of the two simulations. Both the WALE model and the localized dynamic model under predict C'_L , but there is no consistent trend among the Smagorinsky's models: ACE1 overpredicts C'_L , while Flu1 and CFX1 underpredict this quantity.

In conclusion, ACE2 and Flu2, both based on the dynamic model, appear to provide the best agreement regarding the important global quantities. The two other models tested here, in simulations ACE3 and Flu3, provide reasonable agreement in all global quantities, but under predict the r.m.s. lift coefficient.

In the remainder of the paper, a detailed comparison is provided with the results of Lyn and Rodi (1994). However, as pointed out in Sohankar et al. (2000), such a comparison should be made with caution. This is because the experimental measurements were made without the use of "end plates" and the prism aspect ratio used in the experiments was relatively small (side = 1 : axial length = 9.75).

3.2 Time-Averaged Quantities

The time-averaged streamwise velocity along the centerline is plotted in Figure 3. The legend is given in Table 2, and it is used in all subsequent figures. The mean recirculation length, which is the point of zero-crossing of the streamwise velocity, has already been discussed. In the near wake region, all simulations tend to overpredict the size of the wake. Of the ACE simulations, ACE2, based on the dynamic model has the best spatial agreement with the experiments. Among the Fluent simulations, Flu2, again based on the dynamic model, has excellent agreement with the experimental data, better than all other simulations. Simulations using the Smagorinsky's model (CFX1, ACE1 and Flu1) consistently overpredict the negative velocity in the wake. The experimental data shows that the velocity levels off quickly at about 4 span lengths to about 60% of the free stream velocity. This trend is not displayed by any of the simulations; All simulations tend to level off at much later distances, to larger values. This has been a common trend in much of the published simulations (at least Sohankar et al. (2000), Rodi et al. (1997) and Voke (1997)). The reasoning behind such a trend is unclear: the SGS model, grid stretching and freestream turbulence may play a part.

Figures 4 and 5 show the variation of the r.m.s. velocities with the streamwise length. These velocities are thus time-averaged representations of the Reynolds stress tensor. Since LES does not explicitly represent the small scales but only represents their effect on the large scales through an SGS model, one cannot expect true agreement between the LES data and the experimental data. In general, the agreement should increase if the higher frequency contribution to the r.m.s. is negligible. Almost all simulations tend to overpredict the r.m.s. streamwise velocity, and underpredict the r.m.s. vertical velocity. This trend (consistent among all simulations) indicates that the larger eddies of the flow, which are explicitly represented, show artificially higher fluctuations in the direction of the mean flow, and smaller fluctuations in secondary directions orthogonal to the mean flow. The spatial

distribution of the r.m.s. streamwise velocity (e.g. the location of the peak) is also likely to be influenced by the mean flow. The Smagorinsky’s solutions of ACE (ACE1) and Fluent (Flu1) show the highest r.m.s. velocities in both the streamwise and vertical directions. A correlation is clearly evident between the r.m.s. streamwise velocity in the wake and the r.m.s. lift on the prism.

The cross term of the time-averaged Reynolds stress $\langle u'v' \rangle$, which is a measure of the anisotropy of the turbulent field, is shown in Figure 6. Among the various quantities discussed in this paper, the cross term of the Reynolds stress is generally the most difficult for any SGS model to accurately reproduce. ACE3 shows excellent agreement with the experimental data, and Flu2 and Flu3 also show good agreement. The central advantage of the localized dynamic model (of ACE3) over the algebraic dynamic models (of ACE2, Flu2) is to capture the “non-local and history effects” of the flow by computing the differential equation for the SGS kinetic energy. From the Figure 6, it appears that this model has a superior ability to predict the cross term of the Reynolds stress, hence providing a better representation of the anisotropy of the flow. ACE1, Flu1 and CFX1 (all using the Smagorinsky’s model) show the poorest agreement with the experimental data. In addition to the magnitude of the cross term of the Reynolds stress, the sign of this term is also important. The sign of this term (along with the velocity gradient of the mean flow) determines the production or loss of turbulent kinetic energy (sometimes referred to as “shear production”). It is important to correctly represent the interaction between the mean flow and the turbulent field, and ACE2, ACE3, Flu2 and Flu3 are superior to the the Smagorinsky’s models in this regard.

3.3 Phase Averaged Quantities

In the original work of Lyn and Rodi (1994), phase definitions were based on the peaks in the pressure signal obtained from a piezoelectric pressure transducer at the center of the prism sidewall. In our simulations, since the wall region is not computed completely, we choose not

to rely on the peaks in the pressure at one point on the prism side wall. On the other hand, peaks in the global lift spectrum, which is an integral of the pressure on all the prism walls, do not directly correspond to a peak in the pressure signal of Lyn and Rodi (1994). Due to this difficulty in demarcating phases the vertical velocity was used as an indicator for phase definition. Each shedding cycle was separated into 20 phase bins and ensemble averaging was performed. Phase 01 was then assigned to the bin with the most agreement (with Lyn and Rodi (1994)) in the vertical velocity and all other phases were numbered successively. In all cases, Phase 01 turned out to be one phase bin beyond the negative peak in the lift time history. This is roughly consistent with Lyn and Rodi (1994) since a peak in pressure on the top face of the prism corresponds roughly to a negative peak in the lift history. Finally, the original idea, that the first half cycle corresponds to an accelerating free stream (adjacent to the top side wall) and the second half corresponds to a decelerating free stream, still holds in our simulation phases.

Figures 7- 12 show the phase averaged streamlines of the flow, depicting Phase 01. Since the numerous vortices in the near wall region are not captured in the calculations, and the streamlines are created from interpolated velocity values on a coarse grid, the region close to the prism walls should be ignored. For reference, corresponding streamline pictures are also shown for the experimental results of Lyn and Rodi (1994) in Figure 13 and the RANS calculations of Lakehal and Thiele (2001) in Figure 14 ³. In general, there is very good qualitative agreement of the simulations with the experiments. Similar figures for Phase 09 are depicted in Figures 15- 20 The experimental results of Lyn and Rodi (1994) are shown in Figure 21 and the RANS calculations of Lakehal and Thiele (2001) in Figure 22. The phase sorted data presented here helps in understanding several features of the flow that cannot be deduced from the time-averaged data only.

³Although this calculation is not an LES, it is among the few published streamline pictures, and hence is reproduced here

One of the attributes of interest in the streamlines for Phase 01, is the location of the streamline on the top of the prism that separates the shed vortex from the free stream. This streamline depicts the amount of vertical oscillation of the wake and a consistent connection is evident with the r.m.s of the lift. Larger oscillations of the wake, as in ACE1 (Figure 7), lead to larger lift coefficients, while smaller oscillations, as in ACE3 and Flu3 (Figures 9 and 12), lead to smaller lift coefficients.

Another attribute of interest for Phase 01 is the location of the same streamline below the prism, that does not get entrained in the wake. Again, a correlation is observable between the location of this streamline and the mean drag on the prism. Cases in which this streamline is closer to the back face of the prism (thus predicting a smaller shed vortex during Phase 01) correspond to cases with higher mean drag forces (ACE1), while the reverse is also true (ACE3)

For Phase 09, it appears that the separating streamline below the prism that is not entrained in the wake is located too far below the prism in ACE1 (Figures 15) but too close to the prism in ACE3 (Figures 9). This correlates well with the corresponding lift coefficients. In general ACE2, Flu2 and Flu3 show the best agreement with the experimental data.

Figures 23 and 24 show the variation of the vertical velocity along the centerline, for phases 01 and 09 respectively. Agreement of the vertical velocity for Phase 01 was used as a method to sort phases. In the near wake, ACE1 clearly predicts more severe values of vertical velocity (both positive and negative), while ACE3 and Flu3 show much smaller values. This is consistent with the over- and under- estimation of the oscillations in the wake for ACE1, and ACE3, Flu3 respectively. ACE2 and Flu2 show excellent agreement for Phase 01, but by Phase 09, the agreement of Flu2 is much reduced.

In addition to Phases 01 and 09, similar figures are shown for two intermediate phases: phase 05 and 15 (Figures 25 and 26). Phases 05 and 15 are among the “accelerating” and “decelerating” phases respectively, since the free stream adjacent to the top prism side walls

accelerates during Phase 05 and decelerates during Phase 15. During these phases also, simulations using the Smagorinsky’s models overpredict the positive and negative vertical velocities. For these phases, the agreement of ACE2 with the experimental data is remarkably good, while none of the other simulations come within close agreement of the experiment.

4 The Effect of Upwind differencing

It is often claimed that first order upwind differencing (applied to the convective term in the standard finite volume formulation) produces artificial dissipation which makes it unsuitable for large eddy simulation (Mittal and Moin, 1997). Two simulations from our study above (ACE1 and ACE2) were recomputed with the addition of 10% upwinding to the differencing scheme of the convective terms. In these simulations the final difference is the sum of 90% contribution from central differencing and 10% contribution from upwind differencing. It should be noted that this technique of “blending” the original difference with upwinding is a default setting in the CFD-ACE code.

Table 3 shows the change in the global quantities of the flow due to the introduction of upwinding. Figures 27 and 28 show the change in the time averaged x-velocity for ACE1 and ACE2, respectively. Figures 29, 30 and 31, 32 show the change in r.m.s. streamwise and vertical velocity, respectively. For completeness, the streamlines of the flow for Phase 01 are shown in Figures 33–36 and Figures 37–40 for Phase 09.

In both cases, on adding upwinding, the Strouhal number is slightly decreased and the r.m.s. lift coefficient is increased (due to larger oscillations of the wake). Another common observation is that the initial time required for the start of vortex shedding is increased.

For the simulation ACE1 the length of the recirculation zone is almost unchanged as is also evident from the streamwise velocity profile in Figure 27. The slight increase in l_r is associated with a slight decrease in the mean drag \bar{C}_D . The small increase also occurs in the

r.m.s. coefficient of the lift, but the change in the r.m.s. velocity fluctuations is negligible. Additionally, the streamline pictures show that vertical deflection of the streamlines due to the formation of the vortex at Phase 01 or 09 is almost negligible.

For the simulation ACE2, the length of the recirculation zone is decreased significantly (see Figure 28), and correspondingly the mean drag coefficient increases. The r.m.s. stream-wise and vertical velocities show considerable increases with the addition of upwinding and this results in the higher r.m.s. lift coefficient. Larger oscillations of the wake are also evident in the streamline pictures for Phase 01 and Phase 09.

One would expect that for a fixed given inlet kinetic energy the addition of numerical dissipation would reduce the actual energy of the flow, possibly leading to smaller fluctuations. However, it is difficult to interpret the above results on the basis of the reduced kinetic energy of the flow alone, since SGS and viscous dissipation also change when the spatial features of the flow change. Calculating the SGS and viscous dissipation is not an easy task in most commercial codes. While estimates of a particular source of dissipation (e.g. numerical) may be obtained by turning off the other sources (e.g. SGS and viscous), such estimates cannot be obtained for the entire length of the calculation. In conclusion, the effect of upwinding on the flow may be summarized as follows:

1. For the Smagorinsky's model (ACE1), most features of the flow remains unchanged, while there was a small increase in the lift coefficient. A possible explanation for this observation is that the incremental dissipation introduced by the upwinding is very small compared to the other (SGS, viscous and numerical) forms of dissipation.
2. For the dynamic model (ACE2), there was a significant change in the flow features. The recirculation zone is shortened, thereby increasing the drag on the prism. The wake oscillates more vertically, leading to higher r.m.s. lift coefficients.

5 Concluding Remarks

Large eddy simulations of the flow across a square prism have been performed using three different commercial codes employing 4 SGS models. The results were benchmarked using the well known test case of Lyn and Rodi (1994). The effect of the addition of upwind differencing was also studied in two of the simulations. The main conclusions drawn through this investigation are:

1. The Strouhal number is not an indicator of an accurate simulation, since an accurate Strouhal number does not translate to accuracy in other features of the flow.
2. The dynamic models (ACE2 and Flu2) provide impressive agreement in the recirculation length and the r.m.s of the lift coefficient, which are the two most important global quantities of the flow
3. The dynamic models (especially Flu2) again provide the best agreement in the time averaged streamwise velocity
4. All simulations tend to over-predict the streamwise velocity fluctuations and under-predict the vertical velocity fluctuations. Higher velocity fluctuations, especially using the Smagorinsky's model, correlate well with higher lift coefficients
5. When the time dependant data is split into phase bins and ensemble averaged, several features of the flow come to light: the vertical oscillation of the wake, the size and position of the shed vortex, etc. In general, Flu2 and ACE2 offer the best spatial prediction of the wake during its different phases. Correlations can be readily made from the spatial structure of the wake during certain phases, and the global time-averaged results of lift and drag.
6. The addition of upwind differencing has marginal effects on the simulations using the

Smagorinsky's model but more dramatic effects on the simulations using the dynamic model. In both cases, the shedding process is slowed down slightly and the oscillation of the wake is increased, leading to artificially higher lift coefficients.

7. Finally, the overall performance of CFX's implementation of the Smagorinsky's model is poor compared to CFD-ACE and Fluent. This is a direct indicator of the internal numerics of the code

Acknowledgement

This study was supported by the Computer Mechanics Laboratory (CML) at the University of California, Berkeley.

References

- P. W. Bearman and E. D. Obasaju. An experimental study of pressure fluctuations on fixed and oscillating square-section cylinders. 119:297–321, 1982.
- C. J. Freitas. Selected benchmarks from commercial cfd codes. *ASME Journal of Fluids Engineering*, 117:208–218, 1995.
- C. Fureby, G. Tabor, H. G. Weller, and A. D. Gosman. Large eddy simulations of the flow around a square prism. *AIAA Journal*, 38(3):442–452, 2000.
- M. Germano, U. Piomelli, P. Moin, and W. H. Cabot. A dynamic sub-grid scale eddy viscosity model. *Physics of Fluids*, A(3):1760–1765, 1991.
- H. Gross. *Off-Track Vibrations of the Read-Write Heads in Hard Disk Drives*. PhD thesis, University of California, Berkeley, 2003.
- W. Kim and S. Menon. A new dynamic one-equation subgrid-scale model for large eddy simulation. In *33rd Aerospace Sciences Meeting and Exhibit*, Reno, NV, 1995.
- S. Kirpekar and David B. Bogy. A comparison of large eddy simulation models for numerical simulation of airflow in hard disk drives. *CML Report*, 04-013, 2004.
- D. Lakehal and F. Thiele. Sensitivity of turbulent shedding flows to non-linear stress-strain relations and reynolds stress models. *Computers and Fluids*, 30:1–35, 2001.
- B. E. Lee. The effect of turbulence on the surface pressure field of a square prism. *Journal of Fluid Mechanics*, 69(2):263–292, 1975.
- D. A. Lyn, S. Einav, W. Rodi, and J.-H. Park. A laser-doppler velocimetry study of ensemble-averaged characteristics of the turbulent near wake of a square cylinder. *Journal of Fluid Mechanics*, 304:285–319, 1995.

- D. A. Lyn and W. Rodi. The flapping shear layer formed by flow separation from the forward corner of a square cylinder. *Journal of Fluid Mechanics*, 267:353–376, 1994.
- I. McLean and I. Gartshore. Spanwise correlations of pressure on a rigid square section cylinder. 41-44:779–808, 1992.
- R. Mittal and P. Moin. Suitability of upwind-biased finite difference schemes for large-eddy simulation of turbulent flows. *AIAA Journal*, 38:1415–1417, 1997.
- F. Nicoud and F. Ducros. Subgrid-scale modelling based on the square of the velocity gradient tensor. *Flow, Turbulence and Combustion*, 62:183–200, 1999.
- C. Norberg. Flow around rectangular cylinders: Pressure forces and wake frequencies. *Journal of Wind Engineering and Industrial Aerodynamics*, 49:187–196, 1993.
- W. Rodi, J. H. Ferziger, M. Breuer, and M. Pourquie. Status of large eddy simulation: Results of a workshop. *ASME Journal of Fluids Engineering*, 119:248–261, 1997.
- J. Smagorinsky. General circulation experiments with the primitive equations, i. the basic experiment. *Monthly Weather Review*, 91:99–164, 1963.
- R. Smirnov, S. Shi, and I. Celik. Random flow generation technique for large eddy simulations and particle-dynamics modeling. *ASME Journal of Fluids Engineering*, 123:359–371, 2001.
- A. Sohankar, L. Davidson, and C. Norberg. Large eddy simulation of flow past a square cylinder: Comparison of different subgrid scale models. *ASME Journal of Fluids Engineering*, 122:39–47, 2000.
- F. Stern, R. V. Wilson, H. W. Coleman, and E. G. Paterson. Comprehensive approach to verification and validation of cfd simulations – part 1: Methodology and procedures. *ASME Journal of Fluids Engineering*, 123:793–802, 2001.

- J. P. Van doormaal and G. D. Raithby. Enhancements of the simple method incompressible fluid flows. *Numerical Heat Transfer*, 7:147–163, 1984.
- E. R. Van Driest. On turbulent flow near a wall. *Journal of Aero. Science*, 23:1007–1011, 1956.
- B. J. Vickery. Fluctuating lift and drag on a long cylinder of square cross section in a smooth and in a turbulent stream. *Journal of Fluid Mechanics*, 25:481–494, 1966.
- P. R. Voke. *Direct and Large Eddy Simulation II*, pages 355–422. Kulwer Academic Publishers, 1997.

6 Tables

Table 1: Global Results

Current Work	$Re/10^3$	St	l_r	\bar{C}_D	C'_D	\bar{C}_L	C'_L
ACE1	22	0.132	1.715	2.422	0.211	-0.09	1.578
ACE2	22	0.132	1.515	2.132	0.138	0.006	1.280
ACE3	22	0.130	1.626	2.044	0.123	0.001	1.056
Flu1	22	0.129	1.604	2.309	0.192	0.027	1.142
Flu2	22	0.130	1.404	2.210	0.213	-0.151	1.373
Flu3	22	0.130	1.554	2.260	0.259	-0.050	1.064
CFX1	22	0.130	2.627	1.931	0.125	-0.01	1.201
Experiments							
Lee (1975)	176	0.122	-	2.05	0.23	-	1.24
Vickery (1966)	100	0.12	-	2.05	0.17	-	1.32 ⁴
Lyn and Rodi (1994)	21.4	0.134	1.38	2.1 ⁵	-	-	-
Bearman and Obasaju (1982)	22	0.13	-	2.1	-	-	1.327 ⁶
Norberg (1993)	13	0.13	-	2.16	-	-	-
McLean and Gartshore (1992)	23	0.13	-	-	-	-	1.3
From Rodi et al. (1997)							
IIS-KOBA	22	0.13	1.22	2.04	0.26	-0.3	1.31
UKAHY1	22	0.13	1.32	2.2	0.14	-0.02	1.01
TAMU1	22	0.13	1.15	2.28	0.2	-0.03	1.37
From Voke (1997)							
DNS ⁷	22	0.133	-	2.09	0.178	0.005	1.45

³For a *smooth* stream with low turbulent fluctuations

⁴The mean drag coefficient was estimated by integrating the momentum flux, based on the mean velocity profile

⁵Original value reported was 1.2, after correcting for blockage

⁶Data based on three shedding cycles only

Table 2: Common Legend for Figures

Simulation	Marker
ACE1	·
ACE2	○
ACE3	×
Flu1	+
Flu2	*
Flu3	◇
CFX1	▽
<hr/>	
Experiments of Lyn and Rodi (1994)	□
<hr/>	
ACE1 with 10% upwinding	▷
ACE2 with 10% upwinding	◁
<hr/>	

Table 3: The effect of 10% upwind differencing

Case	St	l_r	C_D	C'_D	C_L	C'_L
ACE1	0.132	1.715	2.422	0.211	-0.09	1.578
ACE1 with upwinding	0.128	1.778	2.391	0.215	-0.089	1.714
ACE2	0.132	1.515	2.132	0.138	0.006	1.280
ACE2 with upwinding	0.127	1.169	2.428	0.225	-0.003	1.711

7 Figures

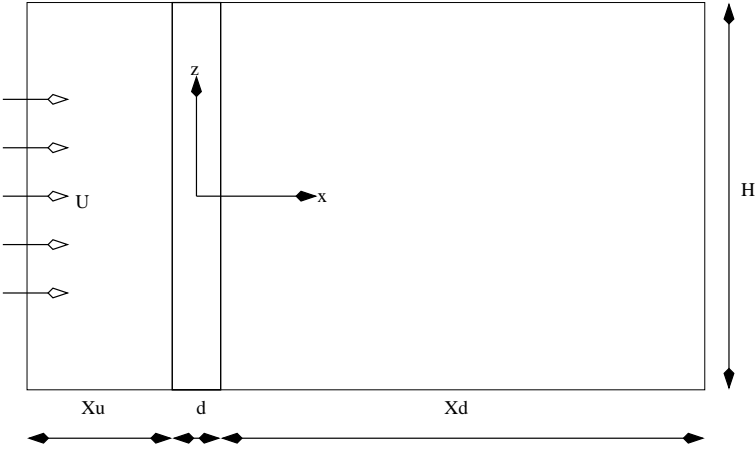


Figure 1: Model Configuration and Setup

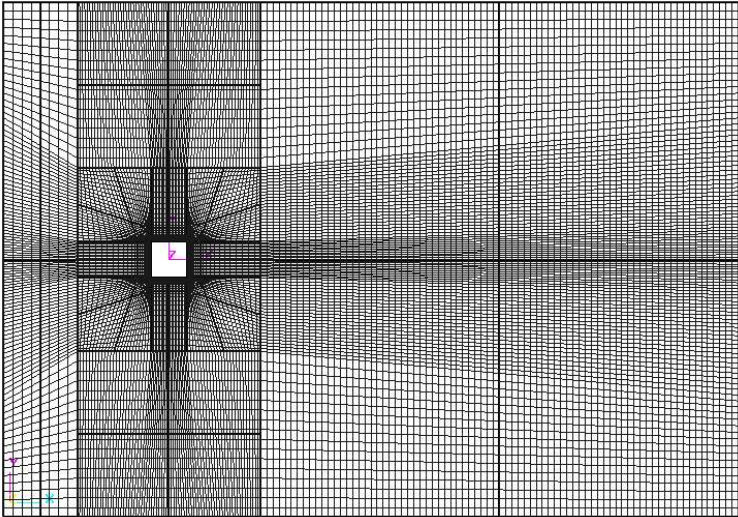


Figure 2: Cross Section of the Grid in the x-y plane. The grid is uniform in the axial (z) direction

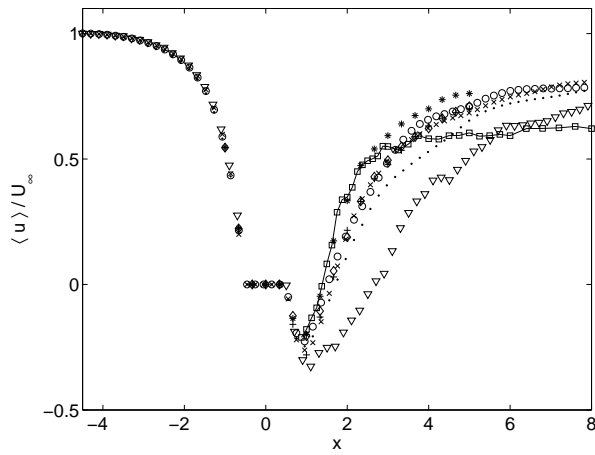


Figure 3: Time averaged streamwise velocity, non-dimensionalized by the free stream velocity U_∞ . See Table 2 for legend

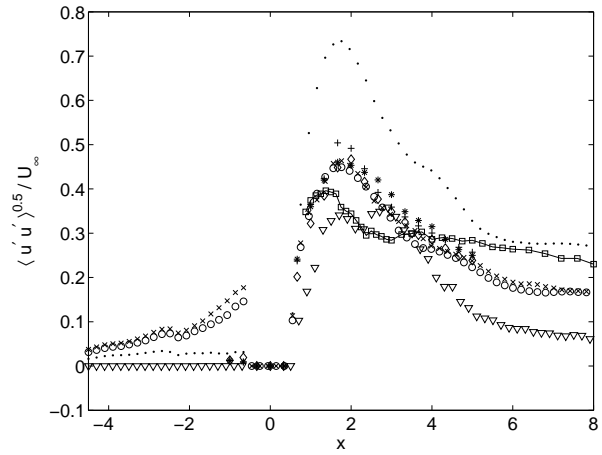


Figure 4: Time averaged RMS streamwise velocity, non-dimensionalized by the free stream velocity U_∞ . This is also the square root of the (1,1) normal Reynolds stress. See Table 2 for legend

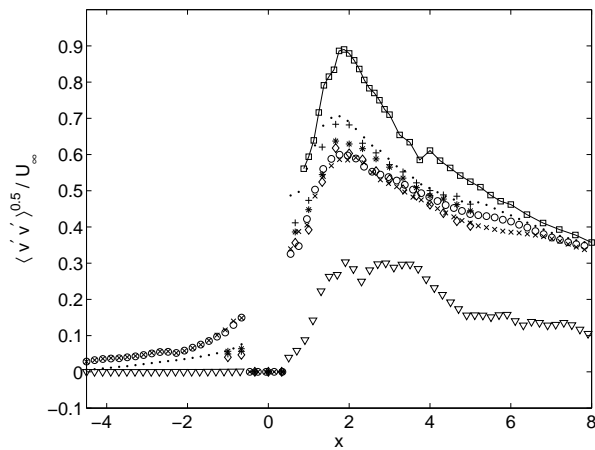


Figure 5: Time averaged RMS vertical velocity, non-dimensionalized by the free stream velocity U_∞ . This is also the square root of the (2,2) normal Reynolds stress. See Table 2 for legend

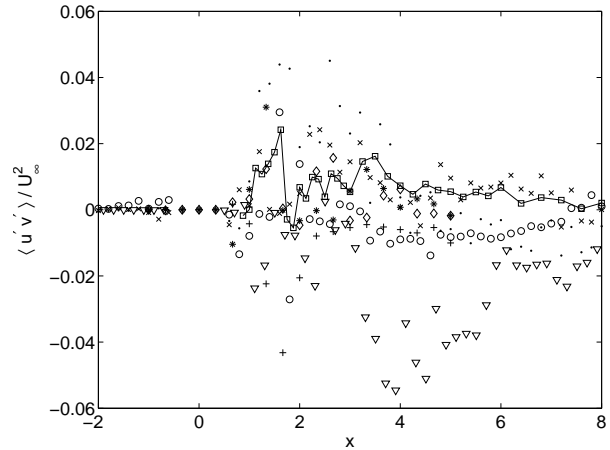


Figure 6: Time averaged cross term (1,2) of the Reynolds stress tensor, non-dimensionalized by U_∞^2 . See Table 2 for legend

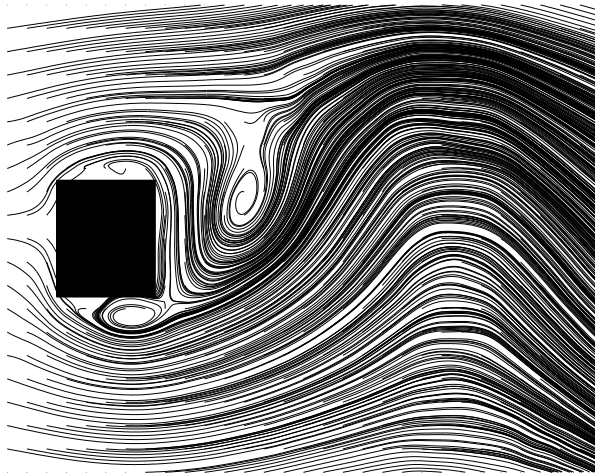


Figure 7: Streamlines for Phase 01, ACE1

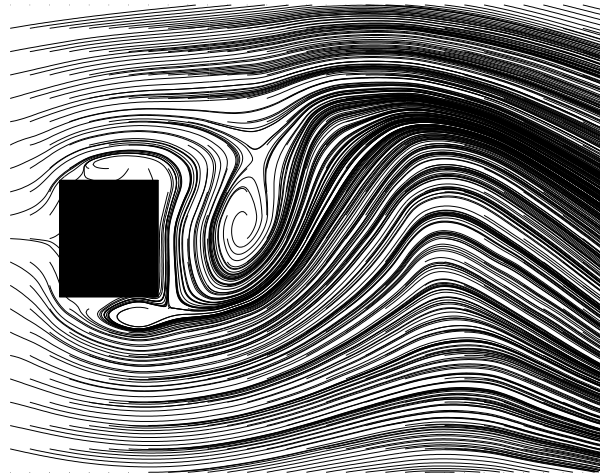


Figure 8: Streamlines for Phase 01, ACE2

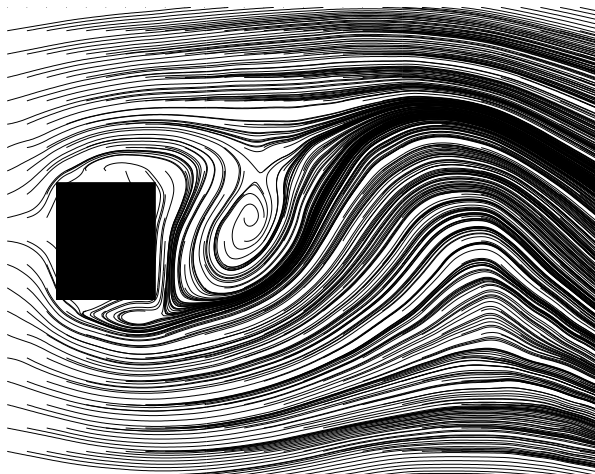


Figure 9: Streamlines for Phase 01, ACE3

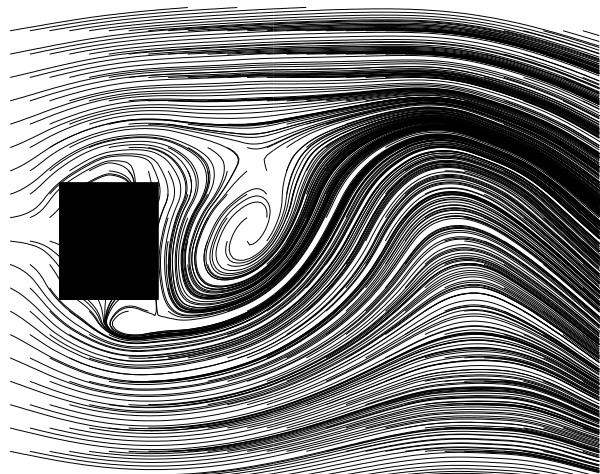


Figure 10: Streamlines for Phase 01, Flu1

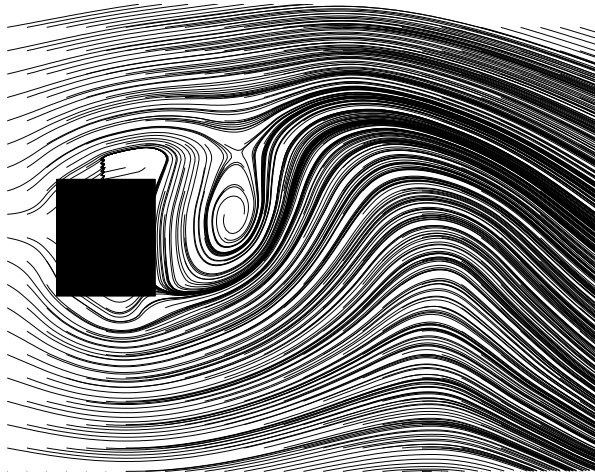


Figure 11: Streamlines for Phase 01, Flu2

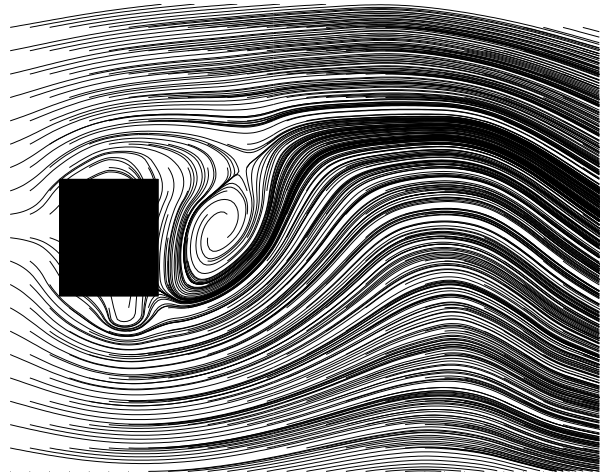


Figure 12: Streamlines for Phase 01, Flu3

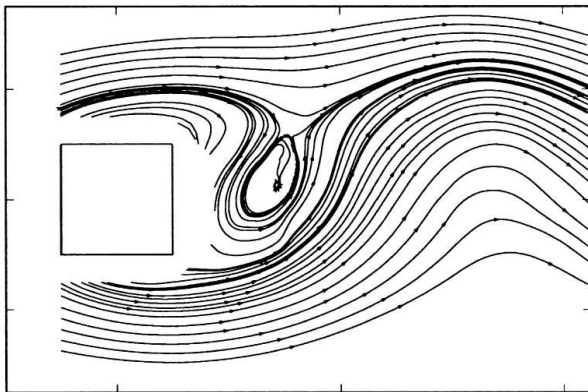


Figure 13: Streamlines for Phase 01, Lyn and Rodi (1994)

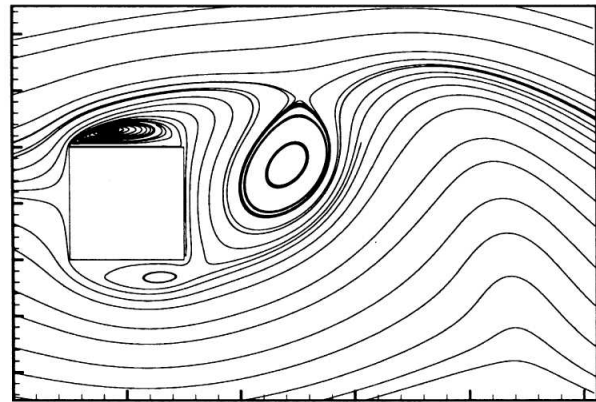


Figure 14: Streamlines for Phase 01, from Lakehal and Thiele (2001)

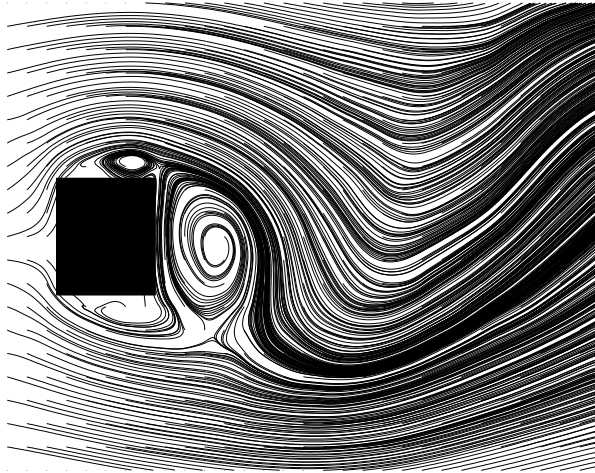


Figure 15: Streamlines for Phase 09, ACE1

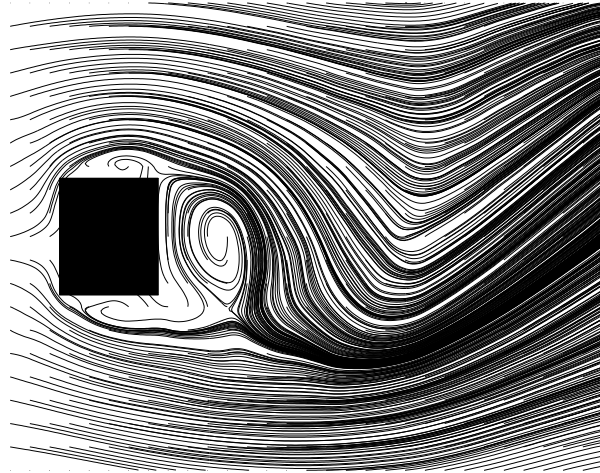


Figure 16: Streamlines for Phase 09, ACE2

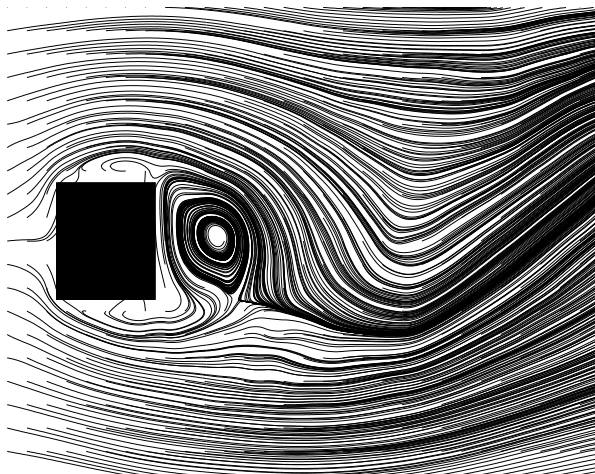


Figure 17: Streamlines for Phase 09, ACE3

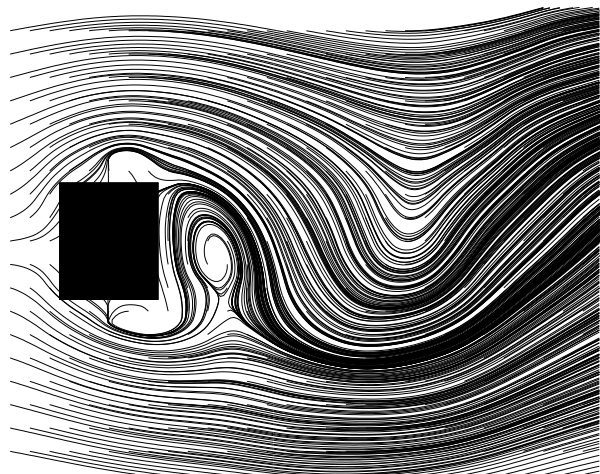


Figure 18: Streamlines for Phase 09, Flu1

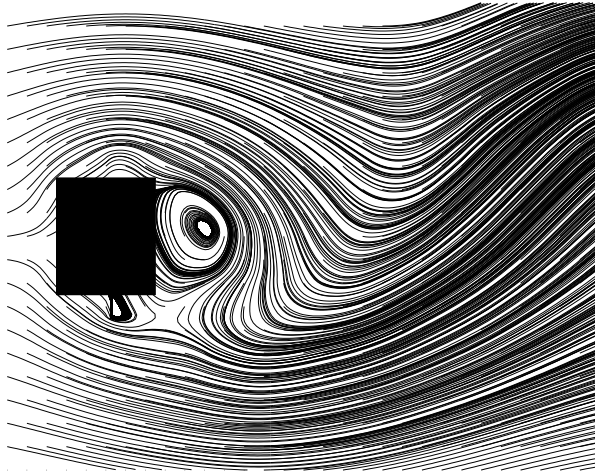


Figure 19: Streamlines for Phase 09, Flu2

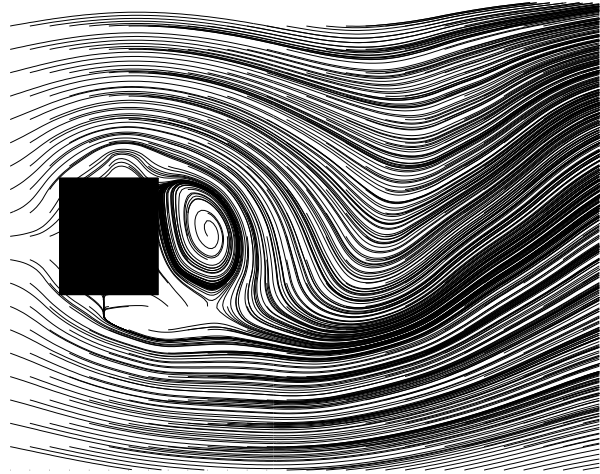


Figure 20: Streamlines for Phase 09, Flu3

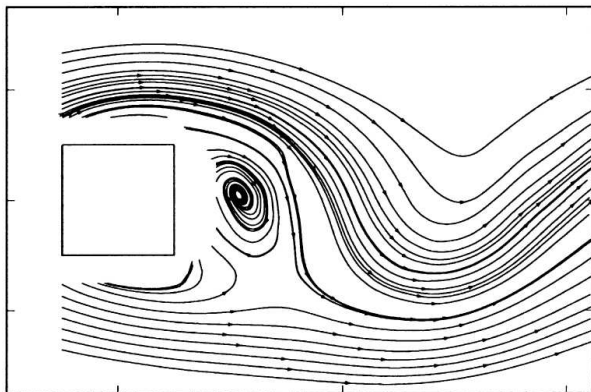


Figure 21: Streamlines for Phase 09, Lyn and Rodi (1994)

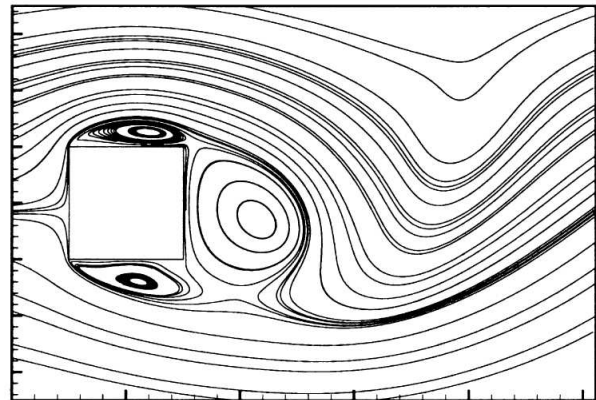


Figure 22: Streamlines for Phase 09, from Lakehal and Thiele (2001)

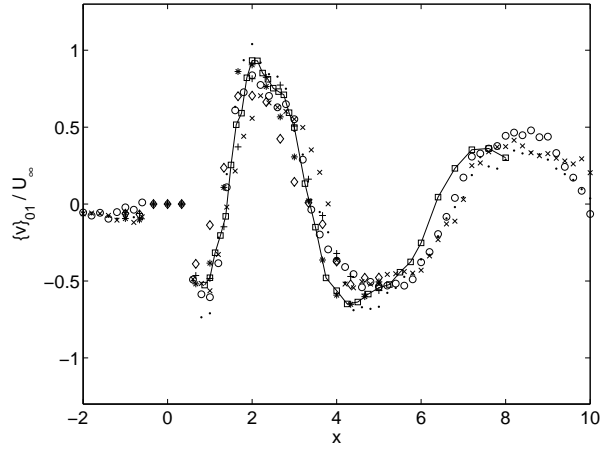


Figure 23: Phase averaged vertical velocity for Phase 01, non-dimensionalized by U_∞ . See Table 2 for legend

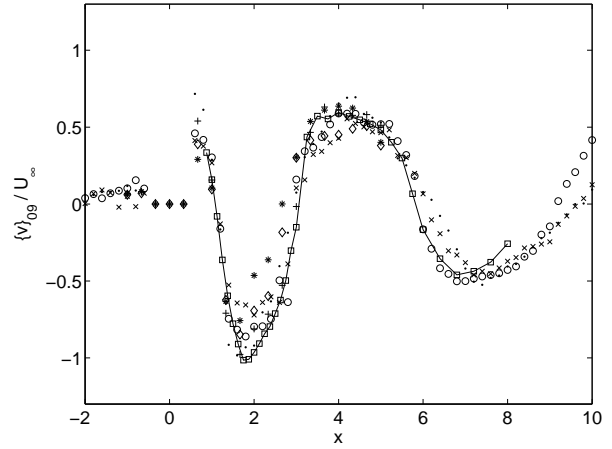


Figure 24: Phase averaged vertical velocity for Phase 09, non-dimensionalized by U_∞ . See Table 2 for legend

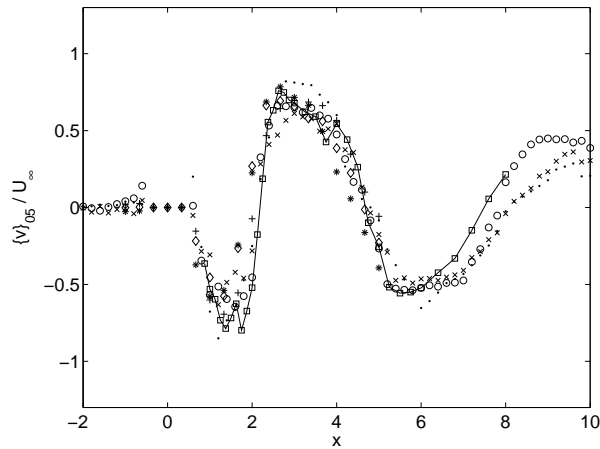


Figure 25: Phase averaged vertical velocity for Phase 05, non-dimensionalized by U_∞ . See Table 2 for legend

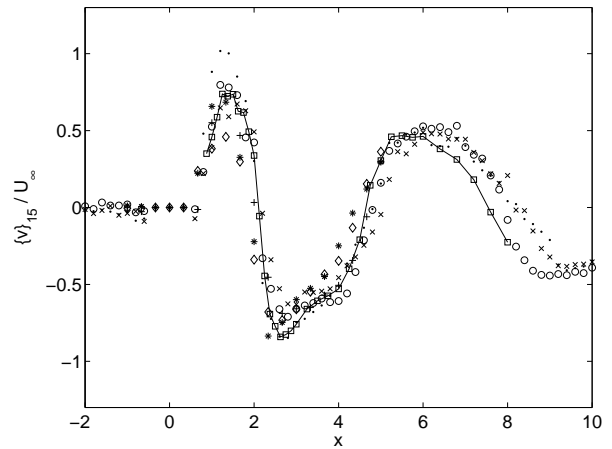


Figure 26: Phase averaged vertical velocity for Phase 15, non-dimensionalized by U_∞ . See Table 2 for legend

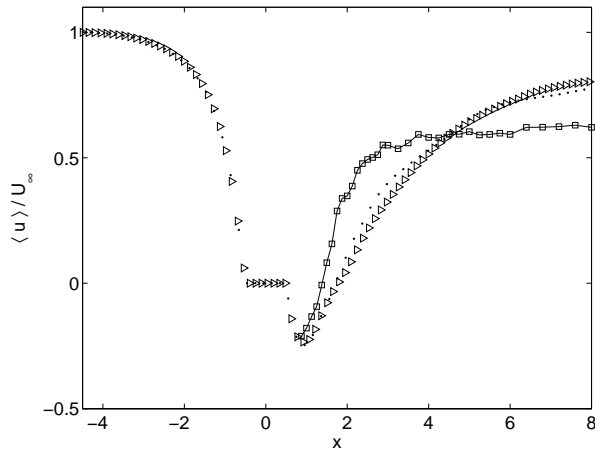


Figure 27: Comparison of time averaged streamwise velocity between ACE1 and ACE1 with 10% upwind differencing. See Table 2 for legend

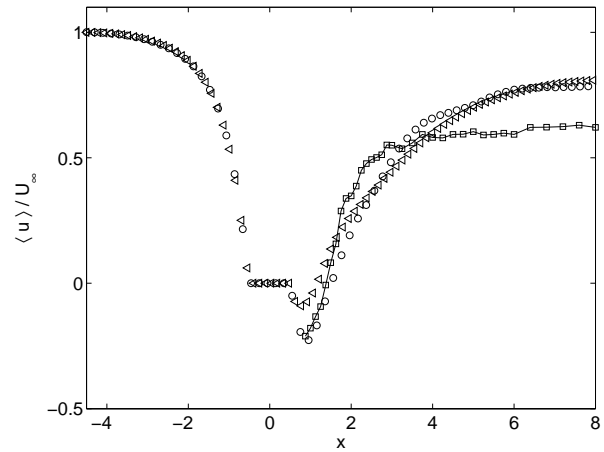


Figure 28: Comparison of time averaged streamwise velocity between ACE2 and ACE2 with 10% upwind differencing. See Table 2 for legend

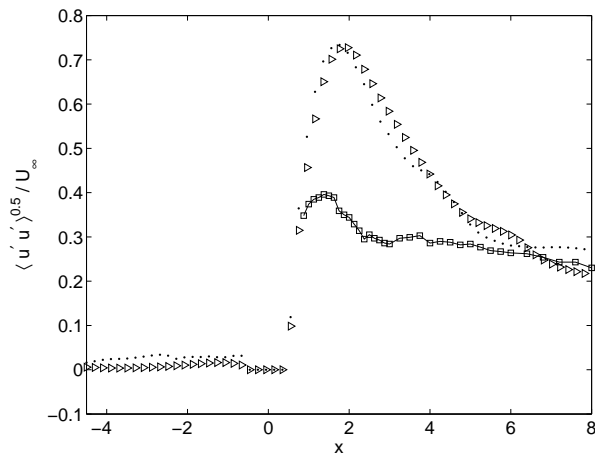


Figure 29: Comparison of time averaged RMS streamwise velocity between ACE1 and ACE1 with 10% upwind differencing. See Table 2 for legend

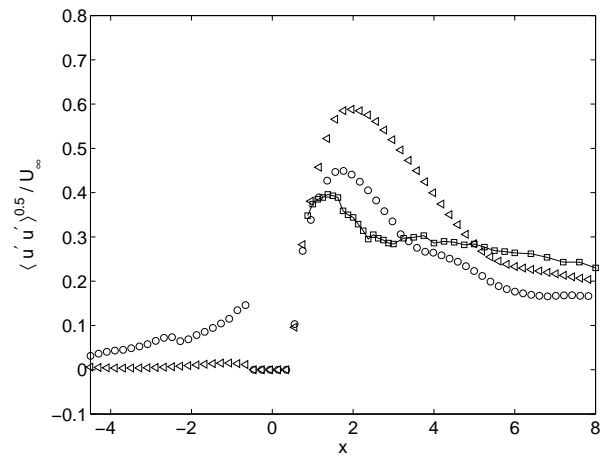


Figure 30: Comparison of time averaged RMS streamwise velocity between ACE2 and ACE2 with 10% upwind differencing. See Table 2 for legend

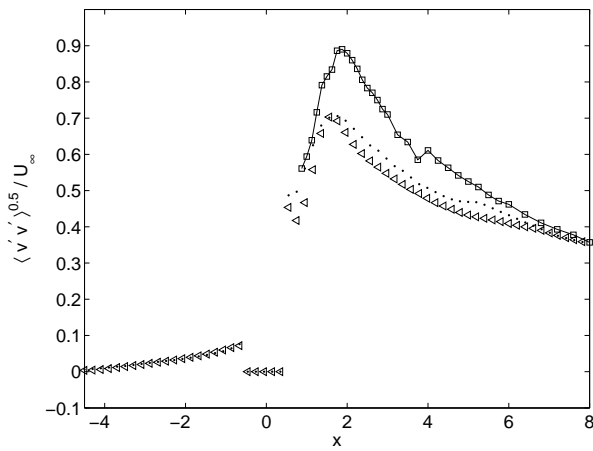


Figure 31: Comparison of time averaged RMS vertical velocity between ACE1 and ACE1 with 10% upwind differencing. See Table 2 for legend

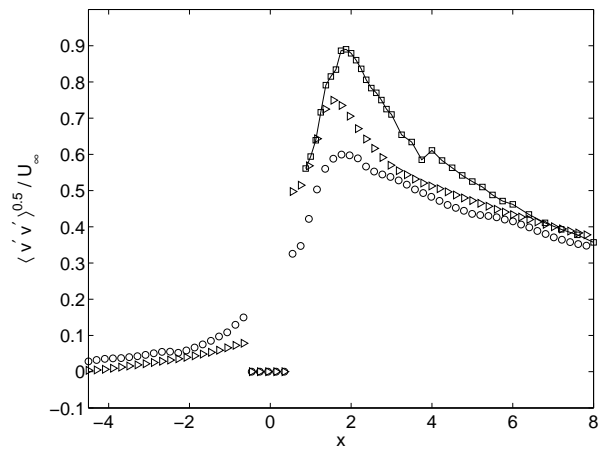


Figure 32: Comparison of time averaged RMS vertical velocity between ACE2 and ACE2 with 10% upwind differencing. See Table 2 for legend

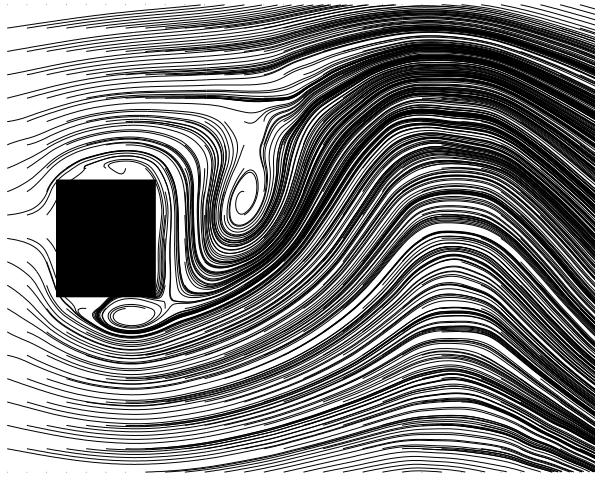


Figure 33: Streamlines for Phase 01, ACE1

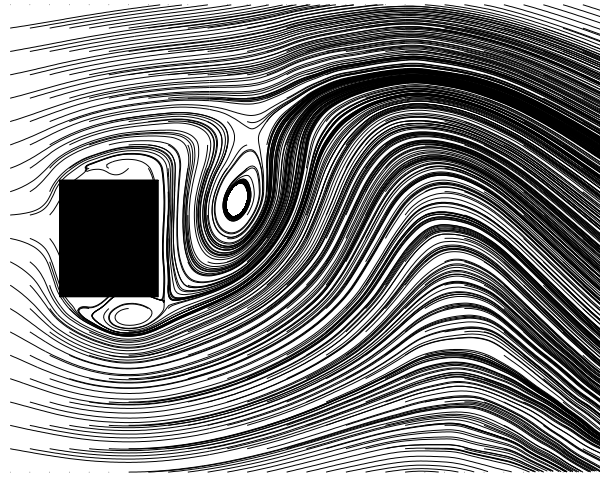


Figure 34: Streamlines for Phase 01, ACE1 with 10% upwinding

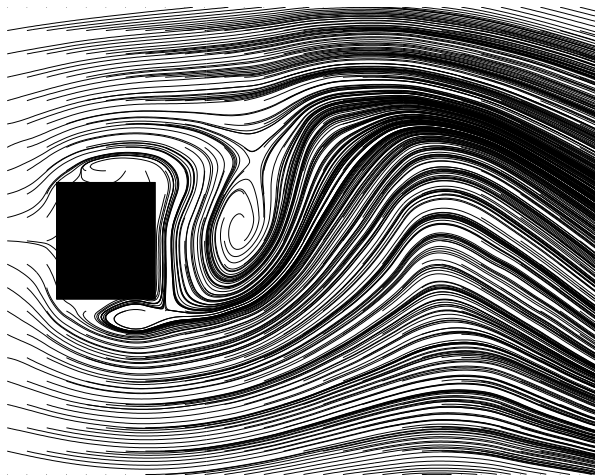


Figure 35: Streamlines for Phase 01, ACE2

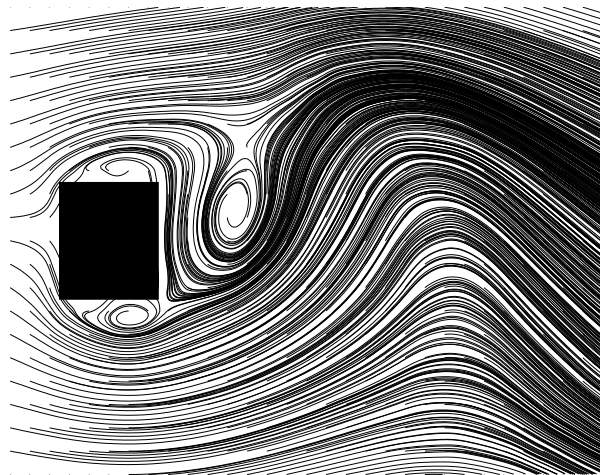


Figure 36: Streamlines for Phase 01, ACE2 with 10% upwinding

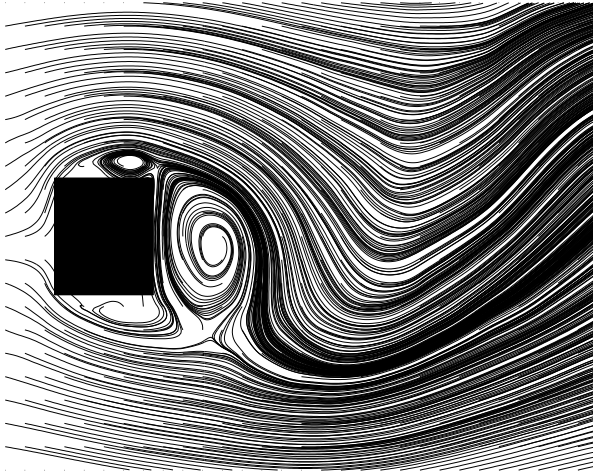


Figure 37: Streamlines for Phase 09, ACE1

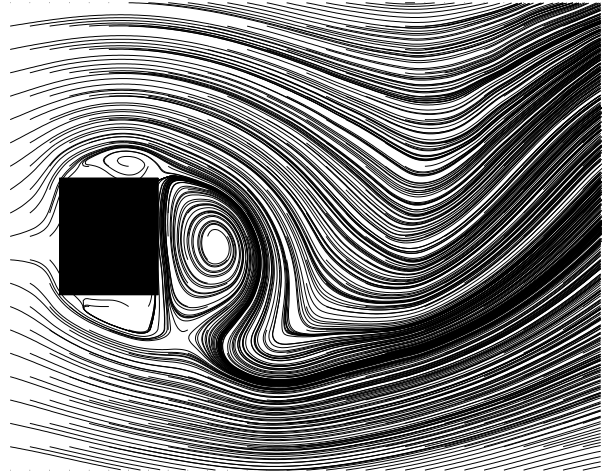


Figure 38: Streamlines for Phase 09, ACE1 with 10% upwinding

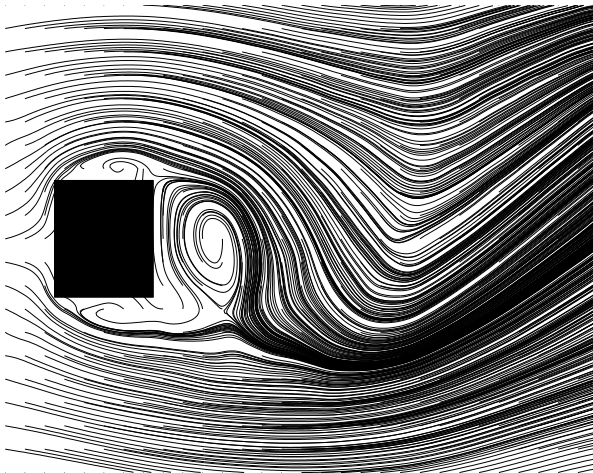


Figure 39: Streamlines for Phase 09, ACE2

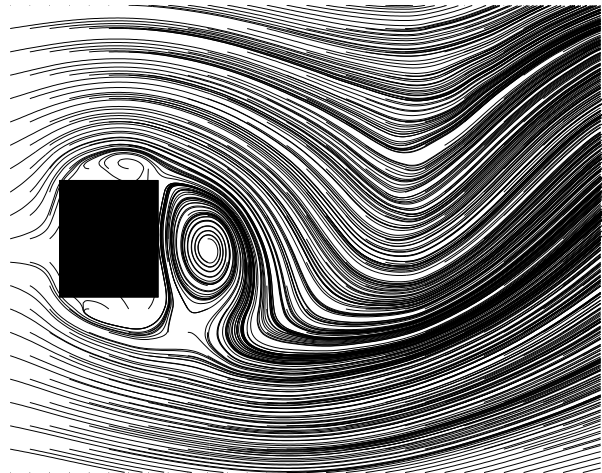


Figure 40: Streamlines for Phase 09, ACE2 with 10% upwinding